IEEE Sensors Applications Symposium
Ottawa, Ontario, Canada, July 2023

Continuous Surface Electromyography and Bioimpedance Sensing from the Same Electrodes

Soumyajyoti Maji*, Sebastian Roubert Martinez* and Robert D. Howe
John A. Paulson School of Engineering and Applied Sciences, Harvard University
Boston, MA 02134 USA
smaji1@seas.harvard.edu, sroubertmartinez@g.harvard.edu and howe@seas.harvard.edu

***Abstract*— Surface electromyography (EMG) for estimating neuromuscular activation suffers from several confounds, including changes in electrode-skin conditions due to contact pressure variation, sweat, and dehydration. These conditions lead to variation in bioimpedance across skin locations and thus variation in the EMG voltages measured at skin electrodes. This paper presents a system that combines standard EMG measurements with continuous bioimpedance sensing using only the electrodes already necessary for EMG. State of the art techniques for simultaneous EMG/Bioimpedance require two extra electrodes for bioimpedance sensing, away from the area of muscle activation. The key to our approach is stimulating the skin-electrode interfaces with voltage frequencies well above native EMG signals. By combining analog circuits, digital signal processing, and analytic calculations using bioimpedance principles, the system can decouple the intertwined signals. We provide design rationales for our system and benchtop characterizations to show accurate bioimpedance measurements (R^2~0.96) under varying simulated EMG signals. We demonstrate system utility in vivo during controlled force generation tasks where controlled alteration to subjects' skin-electrode conditions produce changes in both EMG and bioimpedance. This work provides a basis for continuous, simultaneous EMG and bioimpedance sensing, so impedance variations can be used to normalize EMG signals for improved muscle effort estimates.**

Keywords—electromyography, bioimpedance, analog circuit design, multi-modal wearable bioelectronics

I. Introduction

Surface electromyography (EMG) enjoys widespread use in medicine [1], wearable robotics [2], prosthetic control [3], and sports biomechanics [4]. The EMG voltage sensed at the skin is a function of the 1) combined action potentials from motor unit discharge, 2) impedance of the surrounding biofluids/tissues, and 3) impedance at the skin-electrode interface [5]. While EMG serves as an effective non-invasive measure of neuromuscular activation, it suffers from several confounds, including variability due to skin state [6], muscle fatigue [7], and electrode quality [8]. Of particular interest for continuous monitoring applications is the influence of the skin-electrode electrical impedance on EMG amplitude. This impedance changes during physical activity due to contact pressure variation between the skin and electrodes and due to sweat or skin dehydration, where changes in fluid/salinity can alter electrical resistance. But consistency in impedance is key for reliable EMG [8]. The result is that changes in measured EMG voltage amplitude are due to a combination of changes in muscle activation and bioimpedance variation.

To account for such undifferentiated changes, a simple method is to use separate sets of skin electrodes for EMG and impedance signals, e.g. [9, 10, 17, 18, 19] (see Table I). Using separate electrodes for each of measurement, however, means the measurements are from different anatomical regions, and does not account for differing skin conditions (e.g. contact pressure and sweat levels) at each electrode. It would be preferrable to continuously measure the impedance at the skin contact as well as EMG from the same electrodes.

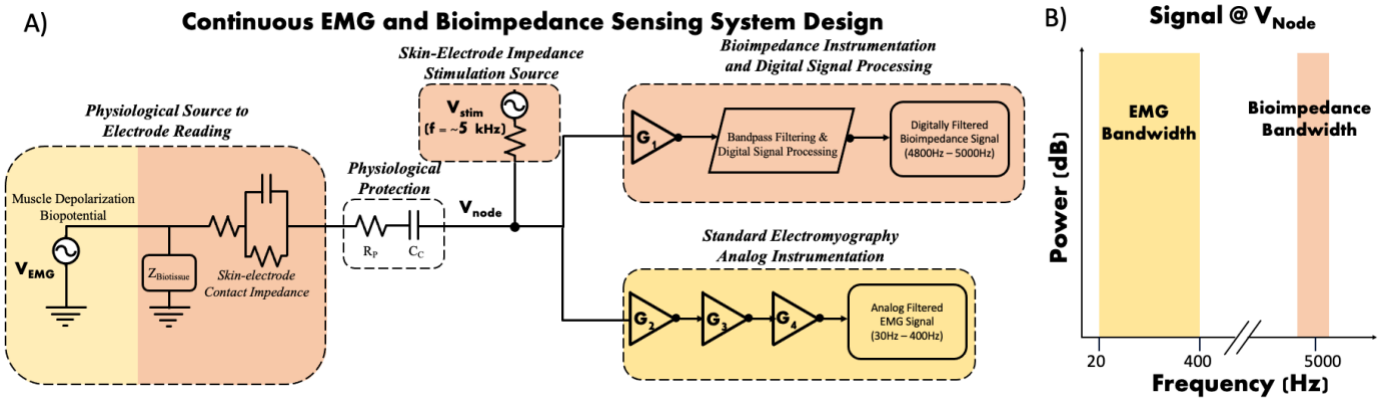

Fig. 1 A) Block diagram of the proposed system design. Yellow shading indicates EMG signal components, while orange indicates bioimpedance components. V_{node} is the key junction of the design as it comprises both the native EMG signal and the injected bioimpedance signal. B) Frequency ranges that enable decoupling of the EMG signal and bioimpedance measurement.

*These authors contributed equally. Funding provided by the National Science Foundation Graduate Research Fellowship, Harvard Graduate Prize Fellowship, Harvard School of Engineering, and the Harvard Move Lab.

Table I. State of the Art Electrode Configurations and Applications for Bioimpedance and EMG

Ref.	Electrodes	Signals	Same Electrodes	Application
[10]	4 total (2 for EMG, 2 for impedance), 0 ground electrode	1 EMG, 1 impedance	No	Loaded knee extension tracking
[9]	4 total (2 for EMG, 2 for impedance), 0 ground electrode	1 EMG, 1 impedance	No	Hand gestures
[17]	4 total (2 for EMG, 2 for impedance), 0 ground electrode	1 EMG, 1 impedance	No	Grip force tracking, hand gestures
[18]	4 total (2 for EMG, 2 for impedance), 0 ground electrode	1 EMG, 1 impedance	No	Unloaded wrist flexion tracking
[19]	7 total (2 for EMG, 4 for impedance), 1 ground electrode	1 EMG, 1 impedance	No	Bicep contraction, no load
This work	**3 total (2 for EMG and impedance), 1 ground electrode**	**1 EMG, 2 impedance**	**Yes**	**Grip force tracking**

In this work, we present a system that combines analog instrumentation, digital signal processing, and fundamental bioelectrical characteristics to enable electromyography measurements while also estimating the bioimpedance at each electrode. This approach leverages the fact that useful EMG signals are largely confined to frequencies below approximately 400 Hz. The circuit probes the skin-electrode interface with a simple battery-powered oscillator at a relatively high frequency (5 kHz) outside of the bandwidth of EMG, and then measures the voltage drop in this high frequency range to estimate skin-electrode impedance.

The next section of this paper describes the design strategy. Careful configuration of the circuitry is required to meet the bioelectrical constraints of EMG and bioimpedance measurements, as well as safety constraints and input characteristics of operational amplifiers. We then present benchtop tests that show that this approach can accurately measure impedance in the presence of simulated EMG signals across a range of amplitudes. These benchtop characterizations include changing potentiometers in real-world settings (not inside a shielded box and far away from the analog electronics) as a ”stress test” emulating real-world human use. Utility of the system is then demonstrated in vivo as subjects generate prescribed forces. To simulate sweat, physiological saline is added to a single electrode (the other skin-electrode interface remains fixed as a control), resulting in a higher EMG signal-to-noise ratio despite the same force generation, due to the lower impedance of the skin-electrode contact, which is also measured. Collectively, the proposed approach extends the capabilities of EMG configurations by measuring one of the confounds of EMG (changing skin state) at multiple skin sites, allowing more targeted impedance measurements at the area of muscle activation. This system enables scalable multi-modal wearable bioelectronics sensing without extra EMG electrodes or interfering with the native EMG signal.

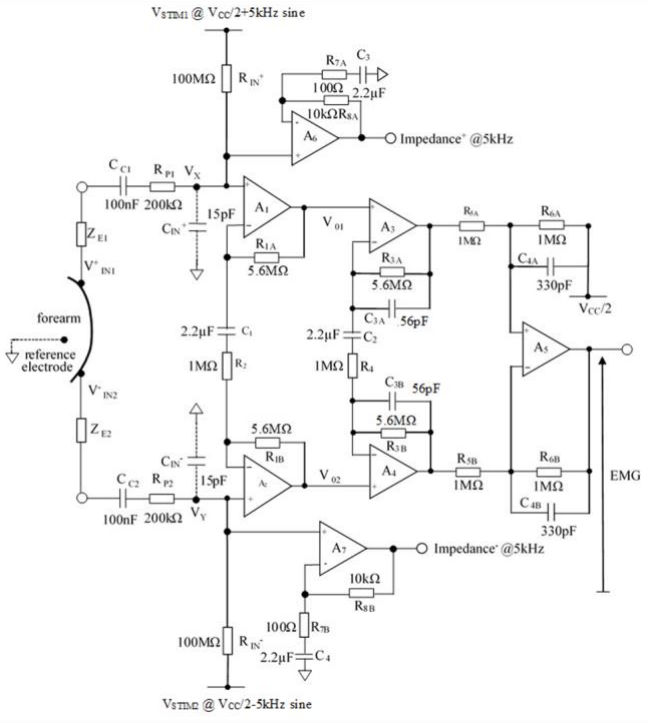

Fig. 2. Schematic diagram combining a multistage EMG amplifier with skin impedance measurements at 5kHz. This diagram shows each electrode lead on the forearm, V_{IN}^+ and V_{IN}^- with high frequency input stimulation voltage V_{STIM1} and V_{STIM2}. Not shown is that ground is connected to both a bony extrusion of the human participant and the negative terminal of the battery power supplies. OPA2132 has been used for op-amps A_1 and A_2. All other op-amps uses OPA2333. Resistors have ±5% tolerance and capacitors have ±20% tolerance unless otherwise indicated.

II. DESIGN

A. Overview

This work proposes a novel system design that enables continuous, simultaneous recording of EMG signals and bio-impedance measurements from the same electrodes. The key concept is the use of different frequency ranges to decouple the EMG signals at 30-400 Hz from bioimpedance measurements at 5 kHz. This approach is complicated by the constraints of the application, which include the low amplitude and relatively high impedance of EMG signals, and the need to maintain bandwidth at both EMG and bioimpedance frequency ranges. There is also a safety requirement to provide DC electrical isolation (i.e. a blocking capacitor) between the user and the electronics. In addition, high input impedance op amps have input capacitances that become limiting under the above constraints.

A functional block diagram for the design is shown in Fig. 1. The portions of the diagram highlighted in yellow correspond to electromyography instrumentation, which is based on a standard differential amplifier for bipolar EMG; the portions in orange correspond to the bioimpedance instrumentation. A 5 kHz

oscillator (a decade higher than EMG frequencies) for impedance measurement is connected to the skin electrode through a series of circuit elements, forming a voltage divider. The signals from EMG and the 5 kHz stimulation mix at V_{node}. The skin-electrode impedance stimulation source is in series with a large common-mode resistor (100 MΩ) to provide DC bias and prevent signal attenuation and distortion at low frequencies, where the blocking capacitor disconnects the skin electrode elements. In the bioimpedance block highlighted in orange, we utilize an AC non-inverting gain amplifier having high input impedance to prevent loading effects at V_{node} as we perform downstream digital signal processing. Finally, in series with V_{node} and the bioelectrical interface, we incorporate a physiological protection capacitor to protect the subject in the worst-case fault scenario (e.g. op-amp failures or shorts causing high leakage current).

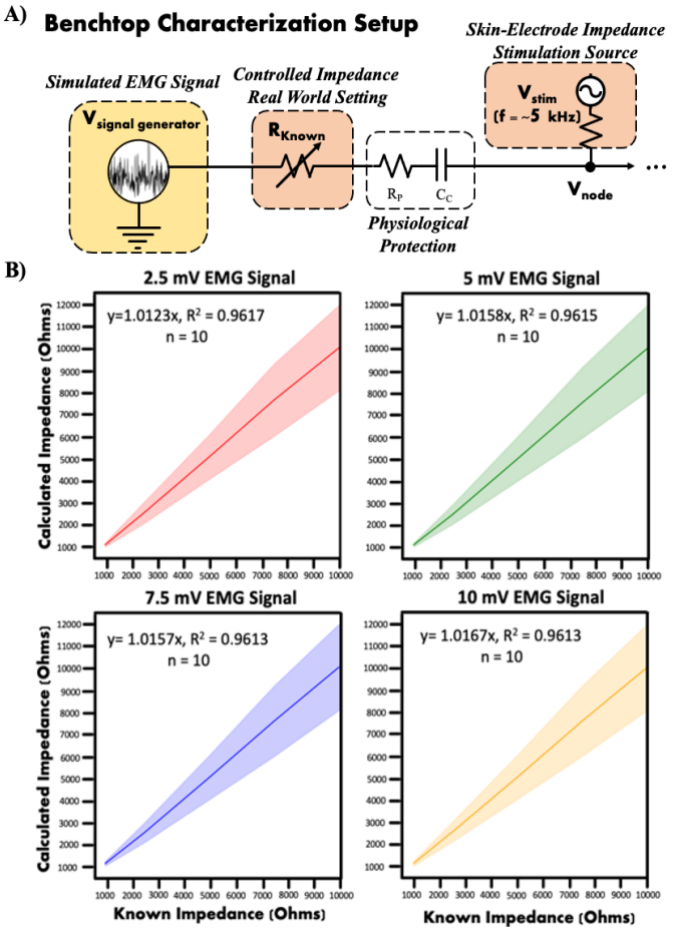

Fig. 3. A) Characterizing performance of proposed approach on the benchtop. A signal generator created a simulated EMG signal. Electrode leads were connected to a potentiometer to provide a precisely controlled resistance. B) Results of characterization for various EMG amplitudes for the same resistance values. Lines are best fits for each EMG signal, shaded regions represent standard deviation of calculated impedance. The variance increases at higher impedances due to capacitor and resistor tolerance creating impedance mismatches that affect op-amp CMRR performance, amplitude shifts at the Wein bridge oscillator, and higher impedance corresponding to higher Johnson-Nyquist noise [15].

B. *Detailed Description*

i) Circuit Operation and Definitions

For EMG measurements, two electrodes are located over the target musculature, while a third reference or ground electrode is placed over a bony prominence which is largely isolated from the EMG biopotentials. Fig. 2 shows the circuit schematic detailing components for bipolar electromyography with bioimpedance measurements for each of the two active electrodes. Z_{E1} and Z_{E2} in Fig. 2 represent each active electrode's combined skin-electrode contact and tissue impedance in the physiological source block in Fig. 1. Through the rest of the manuscript, Z_{E1} and Z_{E2} refer to the positive electrode lead/impedance and to the negative electrode lead/impedance, respectively. V_x and V_y in Fig. 2 represent the key junction, denoted V_{node} in Fig. 1, at the positive electrode and negative electrode, respectively.

ii) Physiological Protection Block

DC blocking capacitors, C_{C1}, C_{C2}, (100 nF) in series with the sensing electrodes Z_{E1}, Z_{E2}, represents the physiological protection block as shown in Fig. 1A. The capacitors prevent continuous flow of DC current from reaching the subject's body. In addition, the current-limiting resistors of 200 kΩ are used in the design so that no more than 30 μA of leakage current across all frequencies reaches the body in a worst-case fault scenario.

ii) Skin-Electrode Impedance Stimulation Source

A 5 kHz sinusoid signal, V_{STIM}, comprises the skin impedance stimulation block as shown in Fig.1A. It is generated using an amplitude-controlled Wein Bridge oscillator. A dual supply op-amp, TLV2471 (Texas Instruments Inc.), powered by a 3.7V battery was used at the oscillator output.

The in-phase sinewave produced by the oscillator is then passed through an unity gain inverting stage, which has a mid-rail DC bias of 1.85V, for single-supply operation. The in-phase sinusoidal signal is fed to the positive electrode Z_{E1} through the common mode input resistor R_{IN}^{+} (100 MΩ) for DC bias and to prevent signal attenuation and distortion at low frequencies. The inverted sinewave component is then fed to the negative electrode, Z_{E2}, via the common-mode input resistor R_{IN}^{-}.

The key function of the stimulation source is to create a voltage divider at high frequencies at V_{node}. At first glance, this voltage divider only relies on the common-input resistors along with Z_{E1} and Z_{E2}, in series with the current limiting resistors R_{P1} and R_{P2}. However, there are additional shunting capacitances at the input terminals of the amplifier, as shown in Fig. 2. These capacitances are mainly contributed by the common-mode input capacitance of the op-amps, C_{IN}^{+} and C_{IN}^{-}, which is 6 pF. In addition, stray capacitance from the prototype stripboard appears in parallel with the common-mode op-amps input capacitance and accounts for 2-3 pF; here we made the conservative assumption of 3 pF. These overall capacitive impedances at 5 kHz result in a 7.5 MΩ impedance that appears in parallel with the current limiting resistor, which is also in series with the sensing electrodes and DC blocking capacitors, C_{C1} and C_{C2}. Therefore, the dominant skin impedance block with the protection resistor fundamentally form a potential divider network with the common-mode input resistor when

driven by the 5 kHz stimulation voltage, V_{STIM}, at each side of the amplifier.

iii) Standard electromyography instrumentation

The first stage of the EMG amplifier, op-amps A_1 and A_2 as shown in Fig. 2, utilizes a dual op-amp, OPA2132 (Texas Instruments Inc.), owing to its high gain bandwidth product of 8 MHz, a very high slew rate of 20V/µs at a supply current of 4 mA/channel, and a high input impedance (10^{13} Ω) to preserve fidelity of the small EMG signal. The second and third stage uses a zero drift, high CMRR (>100 dB), low-voltage offset (10 µV max.) with electromagnetic interference (EMI) filter op-amp (OPA2333, Texas Instruments Inc.), at a quiescent current of 17 µA. This was to ensure that the final EMG output signal has minimal baseline wandering and negligible electromagnetic interference.

The EMG amplifier block shown in Fig. 1A incorporates a modified classic three-stage instrumentation amplifier to record the EMG signals. Most of the low-power op-amps associated with bio-potential measurements, such as the EMG, generally have finite gain bandwidth product. Therefore, it is quite challenging to implement the overall gain to amplify the EMG signals to the desired amplitude level in a single differential stage. Consequently, the gain in this design is distributed equally in two differential stages with a final output stage incorporating a differential to a single-ended conversion. This front-end EMG amplifier in conjunction with the 5 kHz signal generator has a mid-rail DC bias of $V_{cc}/2$ and operates from a single supply coin-cell battery with a nominal voltage of 3.7 V. The overall amplifier gain of 46 dB is distributed equally with 23 dB between the first two stages, while the third stage is primarily used to record the EMG signal. This first stage of the amplifier essentially includes a high-pass filter centered around 0.1 Hz. The second differential stage which is DC coupled to the first so that the output DC bias potentials of the first stage will carry through to the second stage. The second and third stages have low pass filters at 480Hz [16]. Finally, the digitized EMG output signal is digitally filtered in MATLAB, first with a standard high-pass motion filter [11] (corner frequency 20 Hz, slope 12 dB/oct) and then band-pass filtered in MATLAB to 30-400 Hz to extract the desired EMG signal.

iv) Bioimpedance Instrumentation and Digital Signal Processing Block

In the bio-impedance block as shown in Fig. 1A, the EMG signal mixed with the 5 kHz stimulation signal at V_{node} is further amplified (x101 gain) using an AC non-inverting amplifier, A_6 and A_7, with a high input impedance op-amp (OPA2132, Texas Instruments Inc., 10^{13}Ω) to prevent signal attenuation. One of the primary challenges in measuring the 5 kHz impedance signal is the presence of unwanted EMG noise interfering with the low-amplitude impedance signal. This source of interference is generated by the muscle contractions and is developed at the amplifier inputs, V_X and V_Y as shown in Fig. 2. Therefore, a digital band-pass filter at 4.7-5 kHz is used to extract the 5 kHz impedance signal and reject the unwanted external EMG voltages from appearing at both outputs of op-amps A_6 and A_7.

v) Biompedance Analytic Calculations

Following band-pass filtering, the signal appearing at the output of the op-amps A_6 and A_7 as shown in Fig. 2, are first normalized by the gain factor of 101.

Let Z_1 be the overall series impedance constituted by the physiological impedance and physiological protection impedance. Z_1 forms a parallel network with the capacitive impedances of C_{IN}, input terminals of op-amps for electromyography amplification (A_1 and A_2). Z_1 further forms a potential divider network with the common-mode input resistor, R_C. Let the potential divider network at the input of the

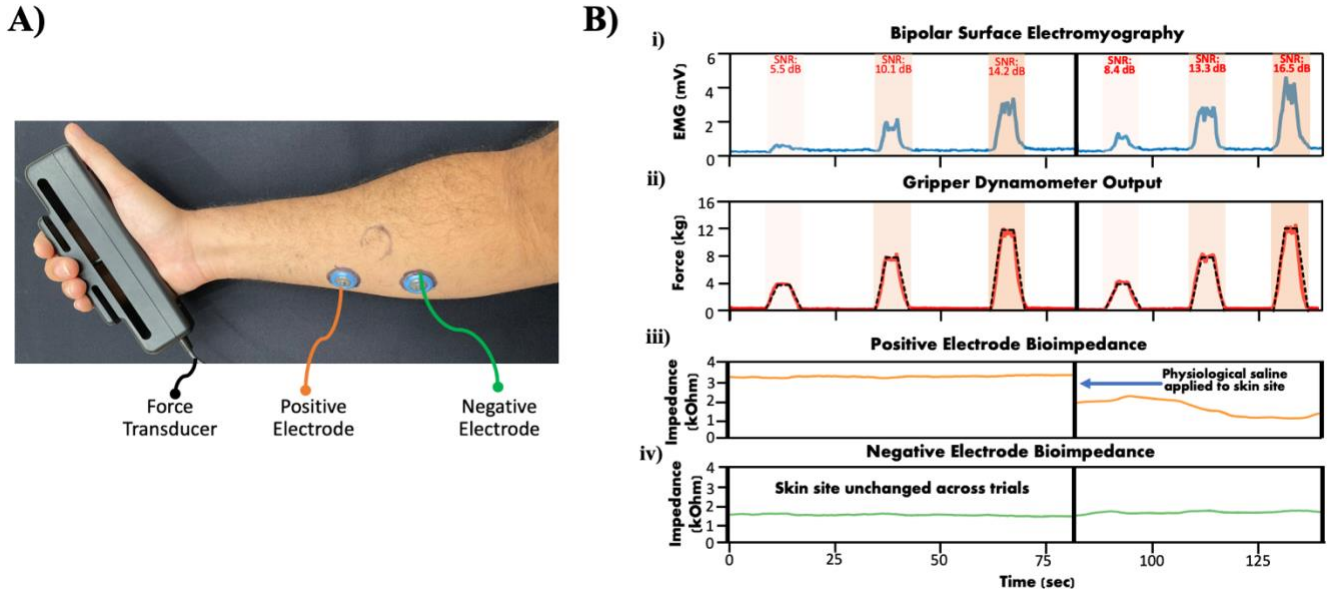

Fig. 4. *In-vivo* characterization of the system in a controlled force generation task. A) Experimental setup on the subject forearm. Two dry electrodes (Neurotrode) were applied to the forearm while a gripper dynamometer records force. (The elbow reference electrode is not shown.) B) Results of the force generation task with physiological saline applied between sets of force-generation trials. The black line in the middle of each recording denotes when saline was applied to the skin site. i) EMG results in blue with signal-to-noise ratio denotes above each contraction. ii) Gripper dynamometer results in red. The target force trajectory is denoted as a dashed black line. iii) Positive electrode bioimpedance. The skin site of this electrode had physiological saline applied across trials. iv) Negative electrode bioimpedance. The skin site of this electrode remain unchanged across trials.

bioimpedance block be defined by an equivalent impedance, Z_{eq}, which can be determined as

$$Z_{eq} = \frac{R_C}{(V_{STIM} - V_{in})} V_{in} \quad (1)$$

where V_{STIM} is the measured output of the Wein bridge oscillator, which must be measured to account for voltage amplitude fluctuations of the stimulation source. Then the series impedance Z_1 is

$$Z_1 = \frac{Z_{eq}^2}{\left[1 - \left(\omega Z_{eq} C_{IN}\right)^2\right]} V_{in} \quad (2)$$

where ω represents the frequency of the skin-electrode stimulation source. Note that all of these are either constant or, in the case of the oscillator output, measured. Thus, the only unknown is a bio-impedance, defined as Z_E,

$$Z_E = \frac{\sqrt{(\omega C_C Z_1)^2 - 1}}{\omega C_C} - R_P \quad (3)$$

where R_P and C_C represent the physiological protection components.

III. Experimental Validation

A. Methods

All analog signals were acquired and synced at 40 kHz with a 16-bit digital acquisition system (PowerLab 35, ADInstruments). The recording input channels were configured with ±2 V range, for a resolution of 62.5 µV at 1.5 LSB. In addition, the channels were AC coupled and utilized a built-in mains filter to minimize power line interference.

i) Benchtop Characterization

To verify the system could adequately measure bioimpedance while EMG signals were received, we performed benchtop measurements as shown in Fig. 3A. At each sensing electrode lead, we connected a dual signal generator (Keysight Technologies, 33500B**)** with output signals corresponding to a simulated EMG signal (white noise with bandwidth of 300 Hz at max amplitudes of 2.5, 5, 7.5 and 10 mV) while connected to resistors of known values (1, 2.5, 5, 7.5, 10 kΩ), similar to literature values of skin impedance at 5 kHz [12, 13]. These benchtop characterizations include changing potentiometer resistance with 1m cables to emulate worst-case real-world conditions. We measured the output of each stimulation voltage source and the sensing leads.

i) In-vivo EMG-Force Task

To verify that decoupling of impedance and EMG signals on the benchtop translates to human applications, we conducted a controlled force generation study while collecting electromyography and bioimpedance, with introduced changes in the electrode impedance. The subject consented to a protocol (IRB23-0164) approved by the Institutional Review Board at Harvard University.

The subject's skin on the forearm and the elbow was cleaned with an alcohol prep. Two dry Ag/AgCl electrodes (Noraxon) were placed on the forearm with a third dry Ag/AgCl electrode (Neurotrode) placed on the bony prominence of the elbow. The two forearm electrodes were connected to the positive and negative bioimpedance sensing leads and the elbow electrode was connected to ground. The outer edges of the electrodes (plastic and non-conductive) were affixed with a skin-safe silicone-based adhesive (Derma-tac, Smooth-On). The subject then held a hand dynamometer (SS25LB force transducer with signals acquired and output by MP35, Biopac Systems, Inc.). All force signals from the dynamometer system were synced using the same equipment described above. The subject viewed a computer monitor displaying force levels sensed by the dynamometer, and instructed to target three increasing force levels (4 kg, 8 kg, 12 kg). The protocol consisted of smoothly ramping up to a target force over 5 seconds, holding the target force for 5 seconds, and smoothly ramping down to no force over 5 seconds, followed by a rest period of about 15 seconds before moving to the next target force level (Fig. 3).

After the first measurement cycle, we removed one of the electrodes from the forearm (positive electrode) and cleaned the skin with an alcohol prep pad and applied approximately 0.3 ml of physiological saline (Sigma Aldrich), which was allowed to run off the skin. We then reapplied the same electrode at the same site and the subject was asked to repeat the force generation protocol described above.

After digitization and initial filtering, EMG data was passed through a root-mean-square (RMS) envelope with 500 ms moving window. Signal-to-noise ratio (SNR) of the RMS EMG was calculated using the built-in snr() function in MATLAB 2022a where the signal was sampled during the approximately 15 seconds of force generation and baseline noise was sampled during rest between trials.

B. Results

i) Benchtop Characterization

The amplitude of the simulated EMG signal did not affect the performance of the impedance sensing (Fig. 3B). At each voltage level (n = 10 each level), the R^2 value ranged between 0.9613 and 0.9617, with a fitted slope ranging from 1.0123 to 1.0167. This confirmed that the impedance estimates were highly independent of the EMG signals.

ii) In-vivo EMG-Force Task

The subject was able to track the force levels prescribed. After the application of physiological saline, the SNR of the EMG signals went up for each respective contraction. Specifically, SNR rises from 5.5 dB, 10.1 dB, and 14.2 dB, to 8.4 dB, 13.3 dB, and 16.5 dB for the 4 kg, 8 kg, 12 kg force levels, respectively. The negative electrode bioimpedance with the unchanged skin site remained virtually unchanged around ~1.5–1.7 kΩ while the positive electrode bioimpedance dropped from ~3.3 to ~1.5 –2 kΩ.

IV. Discussion

The proposed system successfully leverages analog electronics design, digital signal processing, and first principles bioimpedance calculations to decouple surface electromyography signals from bioimpedance measurements using the same electrodes. The benchtop characterization shows that the frequency-based approach enables repeatable bioimpedance calculations robust to signal amplitude swings in the range of native bioelectronic signals. This benchtop characterization was done with impedances in the known range of skin impedance at 5kHz. The in-vivo demonstration of simulating sweat production demonstrates not only how sweat may confound EMG amplitudes for muscle activation but how the system's bioimpedance measurements may help normalize for this confound. Overall, our approach may be generally applicable to other bioelectronic signal sources both invasive

and non-invasive and paves the way for voltage-based in-vivo acquisition of multi-modal bioelectronic signals without the need to alter any existing electrode placement techniques.

One of the key strengths of this design is its ability to decouple the low-frequency EMG signals from the high frequency skin impedance measurements. This was guaranteed by ensuring the skin impedance measurements were made at 5 kHz, which is over a decade above the EMG signal bandwidth (30-400 Hz). The impedance measurements higher than 5 kHz would require a higher gain-bandwidth product or alternatively lower gain of the non-inverting amplifier formed by the op-amps A_6 and A_7 (Fig. 2A). Any impedance measurement below 5 kHz would be challenging as it would be difficult to maintain the integrity of the EMG signals while simultaneously preserving the fidelity of the impedance signal, in the presence of the constraints described above.

The design enables simultaneous measurement of EMG and impedance signals from the same contact electrodes, thereby enabling a simpler design solution requiring only two contact electrodes. The high gain non-inverting amplifier formed by op-amps A_6 and A_7 as shown in Fig. 2A, enable the decoupling of skin impedance measurements at each EMG contact inputs.

A limitation of the proposed approach is variance in the impedance benchtop measurements. This variance could be significantly improved by lowering component tolerance mismatch in capacitors and resistors. Similarly, the design of the stimulation signal source block producing an amplitude fluctuation of about ±2% should be improved for consistent high resolution skin impedance value recording. The design is not suitable for low-power applications as it utilizes FET input op-amps, OPA2132, with supply current of 4 mA/channel. Future work can investigate the use of low-power op-amps to enable wearable monitoring of EMG with bioimpedance.

A limitation of this study is that the sweat production was artificial with application of physiological saline. While we did control for the same skin site, same electrode, and same force, more robust studies of exercise with natural sweat production would provide more conclusive results of the system's utility in long term monitoring and calibration in the fields of medical diagnostics, prosthetics, robot control, and biomechanics.

One possible extension of this work is cross-day validations using machine learning. Recent work [14] showed that ten data-driven models (two polynomial models, eight machine learning models) fit on data with high density EMG arrays to track finger force generation works reasonably well when only validating on the same day as acquisition (best performing model R^2 = 0.866 ± 0.105). But after 3-25 days, model performance significantly degrades (best performing model R^2 = 0.631± 0.172). Extending existing multielectrode arrays with the proposed system may boost this performance for improved human-machine calibration over time and across populations.

V. Conclusion

Electromyography is a useful measure of neuromuscular activation due to its lack of invasiveness combined with low cost and ease of use. However, its many confounds limit its utility for quantitatively estimating muscle activation. This manuscript presents a design to continuously measure one of the EMG confounds, influence of interface impedance on EMG amplitudes, while using the same electrodes used for EMG. By combining analog electronics, signal processing, and first-principles bioelectrical calculations, human exertion estimates may be improved. This may enable better assessments of human intent and force generation in a variety of applications.

Acknowledgment

The authors thank Jonathan Alvarez and Fivos Kavassalis for insightful conversations during development of this work.

References

[1] Benedetti, M. G., Agostini, V., Knaflitz, M., & Bonato, P. (2012). Applications of EMG in Clinical and Sports Medicine. *InTech: Zagreb, Croatia*, 117-130.

[2] D. Novak and R. Riener, "A survey of Sensor Fusion Methods in Wearable Robotics," *Robotics and Autonomous Systems*, vol. 73, pp. 155–170, 2015.

[3] S. Micera, J. Carpaneto, and S. Raspopovic, "Control of hand prostheses using peripheral information," *IEEE Reviews in Biomedical Engineering*, vol. 3, pp. 48–68, 2010.

[4] J. P. Clarys and J. Cabri, "Electromyography and the study of Sports Movements: A Review," *Journal of Sports Sciences*, vol. 11, no. 5, pp. 379–448, 1993.

[5] D. Prutchi and M. Norris, Design and development of medical electronic instrumentation: A practical perspective of the design, construction, and test of Medical Devices. Hoboken, NJ: John Wiley & Sons, 2005.

[6] L. Kalevo, T. Miettinen, A. Leino, S. Kainulainen, H. Korkalainen, K. Myllymaa, J. Toyras, T. Leppanen, T. Laitinen, and S. Myllymaa, "Effect of sweating on electrode-skin contact impedances and artifacts in EEG recordings with various screen-printed AG/agcl electrodes," *IEEE Access*, vol. 8, pp. 50934–50943, 2020.

[7] M. Cifrek, V. Medved, S. Tonković, and S. Ostojić, "Surface EMG based muscle fatigue evaluation in Biomechanics," *Clinical Biomechanics*, vol. 24, no. 4, pp. 327–340, 2009.

[8] J. Heikenfeld, A. Jajack, J. Rogers, P. Gutruf, L. Tian, T. Pan, R. Li, M. Khine, J. Kim, J. Wang, and J. Kim, "Wearable sensors: Modalities, challenges, and prospects," *Lab on a Chip*, vol. 18, no. 2, pp. 217–248, 2018.

[9] R. Kusche and M. Ryschka, "Combining bioimpedance and EMG measurements for reliable muscle contraction detection," *IEEE Sensors Journal*, vol. 19, no. 23, pp. 11687–11696, 2019.

[10] C. Ngo, C. Munoz, M. Lueken, A. Hülkenberg, C. Bollheimer, A. Briko, A. Kobelev, S. Shchukin, and S. Leonhardt, "A wearable, multi-frequency device to measure muscle activity combining simultaneous electromyography and electrical impedance myography," *Sensors*, vol. 22, no. 5, p. 1941, 2022.

[11] C. J. De Luca, L. Donald Gilmore, M. Kuznetsov, and S. H. Roy, "Filtering the surface EMG Signal: Movement artifact and Baseline Noise Contamination," *Journal of Biomechanics*, vol. 43, no. 8, pp. 1573–1579, 2010.

[12] B. B. Murphy, B. H. Scheid, Q. Hendricks, N. V. Apollo, B. Litt, and F. Vitale, "Time evolution of the skin–electrode interface impedance under different skin treatments," *Sensors*, vol. 21, no. 15, p. 5210, 2021.

[13] J. Rosell, J. Colominas, P. Riu, R. Pallas-Areny, and J. G. Webster, "Skin impedance from 1 Hz to 1 MHz," *IEEE Transactions on Biomedical Engineering*, vol. 35, no. 8, pp. 649–651, 1988.

[14] X. Jiang, K. Nazarpour, and C. Dai, "Explainable and robust deep forests for EMG-force modeling" *IEEE Journal of Biomedical and Health Informatics*, pp. 1–12, 2023.

[15] J. D. Rolston, "Closed-loop, open-source electrophysiology," *Frontiers in Neuroscience*, vol. 4, 2010.

[16] V. A. Catacora, F. N. Guerrero, and E. M. Spinelli, "Three-electrode double-differential biopotential amplifier for surface EMG Measurements," *IEEE Transactions on Instrumentation and Measurement*, pp. 1–1, 2023.

[17] A. Briko et al., "A Way of Bionic Control Based on EI, EMG, and FMG Signals," Sensors, vol. 22, no. 1. MDPI AG, p. 152, Dec. 27, 2021.

[18] A. N. Briko, A. V. Kobelev, and S. I. Shchukin, "Electrodes interchangeability during electromyogram and bioimpedance joint recording," 2018 Ural Symposium on Biomedical Engineering, Radioelectronics and Information Technology. IEEE, May 2018.

[19] A. Hafid, S. Benouar, H. Cherrih, B. Ali, and M. K. Talha, "EMG & EIMG measurement for Arm & Hand motions using custom made instrumentation based on Raspberry PI," 2020 2nd (IHSH). IEEE, Feb. 09, 2021.